Spectroscopic studies of Bi^{3+} colour centres in KCl single crystals

1994 J. Phys.: Condens. Matter 6 2101

(http://iopscience.iop.org/0953-8984/6/10/028)

J. Phys.: Condens. Matter 6 (1994) 2101–2116. Printed in the UK

Spectroscopic studies of Bi^{3+} colour centres in KCl single crystals

Jun-Gill Kang†, Hyun-Mo Yoon†, Gang-Moon Chun†, Youn-Doo Kim† and Taiju Tsuboi‡

† Department of Chemistry, Chungnam National University, Daejeon, 305-764, Korea
‡ Faculty of Engineering, Kyoto Sangyo University, Kamigamo, Kyoto 603, Japan

Received 29 July 1993, in final form 13 October 1993

Abstract. Absorption spectra of KCl:Bi^{3+} crystals were measured at various temperatures. Six absorption bands were observed at 335, 245, 212, 207, 201 and 196 nm. The first five bands are assigned to the A, B, C_1, C_2 and C_3 bands and the last to the charge-transfer D′ band. The emission from KCl:Bi^{3+} excited in the A absorption band was measured as a function of exciting photon energy and temperature. The A-band excitation produced two emission bands peaking at 388 and 430 nm, the excitation spectra of which are not the same. The temperature dependence of the decay times is described for the two emission bands. The polarized emission spectrum and the angular dependence of polarization ratios of the A-band emission were also investigated to determine the symmetry axes of the Bi^{3+}-vacancies complex. The results are interpreted in terms of a model in which the reduction effect of the strong spin–orbit interaction on the Jahn–Teller effect coupling to the E_g mode is taken into account. An additional perturbation caused by two cation vacancies is required to present the definitive assignment of the A-band emission from KCl:Bi^{3+}.

1. Introduction

Optical properties of alkali halide crystals containing a small amount of Tl^+-like ions with s^2 electronic configuration have been extensively studied. The Tl^+-like ions exhibit three characteristic absorption bands, designated A, B and C bands in order of increasing energy (Seitz 1938, 1939). These absorption bands are due to transitions from the $(a_{1u})^2$ ground state to terms arising from the $a_{1g}t_{1u}$ configuration in the molecular-orbital scheme: the C band is attributed to the spin-allowed transition $^1A_{1g} \rightarrow {}^1T_{1u}$ and the B band to $^1A_{1g} \rightarrow {}^3E_u$ and $^3T_{2u}$ allowed partially by lattice vibrations. Of the three absorption bands, the A band corresponding to the transition $^1A_{1g} \rightarrow {}^3T_{1u}$, which is forbidden by the spin selection rule, has attracted particular interest. The A band, however, is partially allowed by off-diagonal elements of spin–orbit (SO) interaction between the $^3T_{1u}$ and $^1T_{1u}$ states. In the intermediate scheme, the off-diagonal elements of the SO interaction cause considerable mixing of these two states and result in $^3T^*_{1u}$ and $^1T^*_{1u}$ as follows: $|^3T^*_{1u}\rangle = -\nu|^3T_u\rangle + \mu|^1T_{1u}\rangle$ and $|^1T^*_{1u}\rangle = \mu|^3T_u\rangle + \nu|^1T_{1u}\rangle$, where μ and ν are coupling constants ($\mu^2+\nu^2 = 1$). Besides the three absorption bands, one or two D bands may be found, which are caused by perturbed excitons or charge transfer from halide ions to s^2 ions.

Phosphors excited within the A absorption band produce one or two characteristic emission bands (Fukuda 1970). The results have been interpreted in terms of a model that includes the Jahn–Teller effect (JTE) and the SO interaction. In the framework of the linear JTE with the $E_g(Q_2, Q_3)$ mode, two kinds of minima, tetragonal (T*) and rhombic

0953-8984/94/102101+16$19.50

(nearly tetragonal, X) can coexist on the $^3T^*_{1u}$ adiabatic potential-energy surface (APES) under the intermediate SO interaction. When these two minima are accessible after A-band excitation, the phosphors give rise to two A-emission bands referred to as the A_X and the A_T. (Mugnai *et al* 1982).

In many ways, the study of luminescence of multivalent cations with the s^2 electronic configuration in alkali halide single crystals has just begun. Previously, we reported the A-band emission from Pb^{2+} (Kang *et al* 1985), Ge^{2+} (Kang *et al* 1988) and Sb^{3+} (Choi *et al* 1991) phosphors and proposed the relaxed excited state (RES) responsible for the A-band emission. When a multivalent ion is substituted into an alkali halide lattice, it must be associated with an effect of the charge-compensating cation vacancy (CCV or v_c^-). For the trivalent Sb^{3+} centre, the CCV is expected to be more effective, compared with the cases of divalent Pb^{2+} and Ge^{2+}. Surprisingly, an observable splitting was not found in the A-band absorption and emission spectra from Sb^{3+} ions. According to the polarization spectrum and the angular dependence of polarization ratios of the A_T. emission from Sb^{3+}, the anisotropy arises from the dynamic JT interaction coupling to the E_g mode. It was also found that the JT interaction coupling to the $T_{2g}(Q_4, Q_5, Q_6)$ and the vacancies situated in the next-nearest-neighbour (NNN) and nearest-neighbour (NN) positions to the Sb^{3+} ion give rise to an additional perturbation.

To date, studies of the luminescence of Bi^{3+} colour centres in alkali halide crystals have not been performed, although the ion has been widely used on an optical material owing to its optical characteristics. Only a few papers dealing with absorption of Bi^{3+} ions have been reported (Höner *et al* 1971, Hughes and Pells 1975, Radharkrishna and Srinivasa Setty 1976). In this study, a wide variety of experimental measurements were undertaken to suggest a satisfactory picture of the luminescence mechanism and a comprehensive model for Bi^{3+} ion-doped alkali halide single crystals. These include measurements of the absorption spectrum at various temperatures and the A-band emission as a function of the exciting photon energy and temperature. The time-resolved emission spectrum and the polarization of the A-band emission were also investigated to confirm the proposed model.

We found that, like Tl^+ and Pb^{2+} ions, the Bi^{3+} ion in alkali halide single crystals has a strong SO interaction, giving rise to the reduction effect on the JTE. The primary question was, 'What relaxed excited states are to be expected from the A absorption process?', in the case of strong SO interaction. For the answer, we proposed a theoretical model for the effect of the strong SO interaction on the two kinds of minima on the $^3T^*_{1u}$ APES. For the RES responsible for the A-band emission from KCl:Bi^{3+}, the CCV was taken into account as an additional perturbation.

2. Experimental details

Single crystals of KCl containing about 400 ppm of Bi^{3+} ions were grown under vacuum using the vertical Bridgman method at Chungnam National University (CNU). A thin sample, cleaved from the ingot, was heated at 500 °C for 30 min and rapidly quenched to room temperature before commencing measurements.

Measurements of absorption spectra and time-resolved spectra were carried out at Kyoto Sangyo University (KSU) by using a Shimadzu UV-3100 spectrophotometer and a Hamamatsu Photonics C2830 Streak Camera system in combination with a Molectron UV14 N_2 laser, respectively. The emission and excitation spectra were performed at CNU. For optical measurements at low temperature, the sample was placed on the cold finger of an Air-Product He refrigerator and the temperature of the sample was controlled by using

an APD-B temperature controller. Optical excitation was made by an Oriel Universal Xe arc lamp and a Jobin-Yvon H-20 monochromator. The luminescence was measured at right angles to the excitation with an ARC 0.5 m Czerny-Turner monochromator equipped with a 1200 grooves/mm grating. The detector was a cooled Hamamatsu R-933-14 photomultipler feeding a Pacific photometer. A proper cut-off filter was placed after the sample to eliminate unwanted stray light and high-order emission light. For the polarization measurements, the exciting light was polarized by a Glan-Thomson prism polarizer in a Melles-Griot rotatable mount and the emitted light was passed through an analyser, consisting of a Glan-Thomson polarizer in a similar mount and a quartz quarter-wave plate. Details of the optical arrangements have been given in previous publications (Choi *et al* 1991, Tsuboi and Silfsten 1991).

3. Results

3.1. Absorption spectrum

Absorption spectra of KCl:Bi^{3+} single crystals were measured at various temperatures between 15 and 300 K. As shown in figure 1, three absorption bands are observed at 335, 245 and 190–220 nm. The lowest band appearing around 320–350 nm is very broadened and somewhat insensitive to temperature. The 245 nm band appears as a band at 27.7 K. In contrast, the high-energy band appearing around 190–220 nm shows a very characteristic temperature dependence. At low temperature the 190–220 nm band splits into 212, 207, 201 and 196 nm bands. At low temperature the intensity of the 196 nm band was increased markedly, while the intensities of the first three peaks were not increased so much. This indicates that the 196 nm band may not correlate with the first three peaks. The three peaks seem to compose a triplet band structure. The triplet band structure of KCl:Bi^{3+} is very similar to the cases of KCl:Pb^{2+} (Onaka *et al* 1965, Schmitt 1982) and KCl:Sb^{3+} (Tsuboi *et al* 1992). Our result is also the same as that reported by Höner *et al* (1971). Accordingly, we can assign the 335 nm (3.70 eV), 245 nm (5.06 eV) and the triplet-structured 201–212 nm bands to the A, B and C bands, respectively. Thus, the 212 nm (5.85 eV), 207 nm (5.99 eV) and 201 nm (6.17 eV) bands are attributed to the C_1, C_2 and C_3 components of the C band, respectively. For some phosphors, addition D or D′ bands appear near the fundamental absorption edge, where these two bands are interpreted as a perturbed exciton and an electron transfer from an anion to the positive impurity, respectively. The 196 nm (6.33 eV) band of KCl:Bi^{3+} can be assigned as the D′ band owing to its characteristic temperature dependence.

The A bands of KCl:Sb^{3+} and KCl:Bi^{3+} differ in band structure and temperature dependence. For KCl:Sb^{3+}, with increasing temperature the intensity decreases and the half-width increases. The A band of KCl:Sb^{3+} is nearly one Gaussian band structure (Tsuboi *et al* 1992). For KCl:Bi^{3+} the half-width of the A band is very large, compared with that of KCl:Sb^{3+}. This indicates that the A band of KCl:Bi^{3+} consists of more than two Gaussian bands. It has been suggested that the broad A band is due to overlapping of absorption bands arising from two different ions Bi^{2+} and Bi^{3+} single crystals. For Bi^{2+} ion, transitions $^2P_{1/2} \rightarrow {}^2S_{1/2}$ and $^2P_{3/2} \rightarrow {}^2D_{1/2}$ are expected to be overlapped in the A-band region. These transitions are totally allowed by the electric dipole moment and these absorptions will be observed as very strong. Owing to this selection rule, as well as another factor that the decomposition of $BiCl_3$ to $BiCl_2$ and $BiCl_4$ on increasing the temperature does not take place, we can rule out the coexistence of the two ions in KCl single crystals.

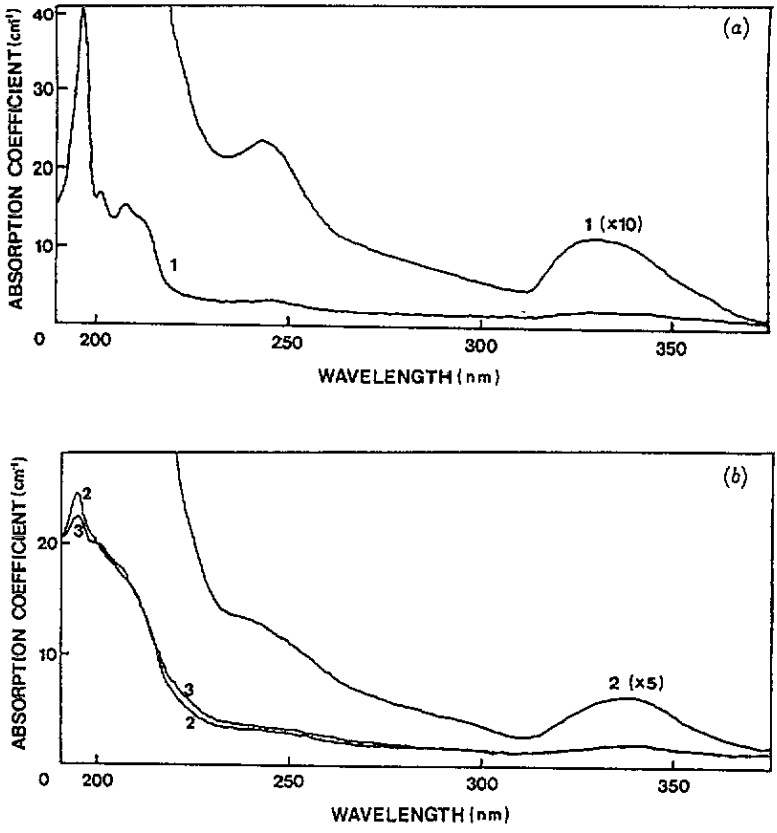

Figure 1. Absorption spectra of KCl:Bi^{3+} single crystals measured at $T = 27.7$ K (1), 230 K (2) and 274 K (3).

In general, the oscillator strength of the B band increases with increasing temperature since the B-band absorption is partially allowed by lattice vibrations. For KCl:Bi^{3+}, an increase of the B-band intensity is not observed. At low temperature, the B-band shape is indistinct, while at high temperature it does not appear clearly. It could be because the broadening of the C band overlaps the weak B band.

3.2. A-band emission spectra and life times

The intensity spectra of the emission from KCl:Bi^{3+} excited within the A absorption band were measured at 16 K. As shown in figure 2, at low temperature the shape of the emission spectrum is very dependent on the exciting photon energy. The 320 nm excitation produces an emission band peaking at 388 nm with a long tail down to 450 nm, while at 325 nm excitation the intensity of the 388 nm emission becomes very strong and it accompanies an additional weak band at its low-energy side. As the exciting photon energy decreases, the intensity of the high-energy emission band decreases and that of the low-energy band increases. At the 335 nm excitation, the high-energy band appears as a trace, while the low-energy band appears as a main band peaking at 388 nm. The excitation spectra of the 388 and 430 nm emission bands were measured at 16 K. As shown in figure 3, the excitation spectra for both emission bands are not the same: the 326 and 334 nm excitations yield the maximum intensities of the high-energy and low-energy emission bands, respectively.

This suggests that the two emission centres could not be equivalent. It can be seen that the combination of the two excitation spectra is similar to the A absorption spectrum covering from 310 to 360 nm.

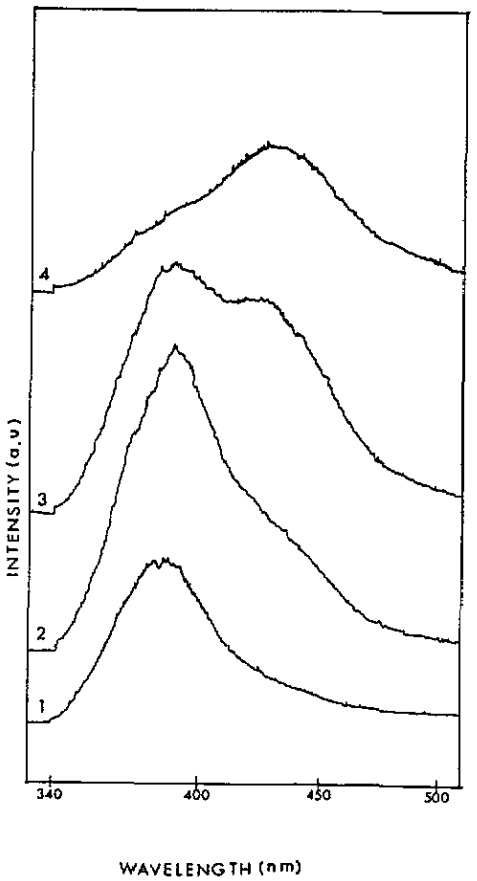

Figure 2. Emission spectra from KCl:Bi^{3+} excited at 320 nm (1), 325 nm (2), 330 nm (3) and 335 nm (4) at $T = 16$ K.

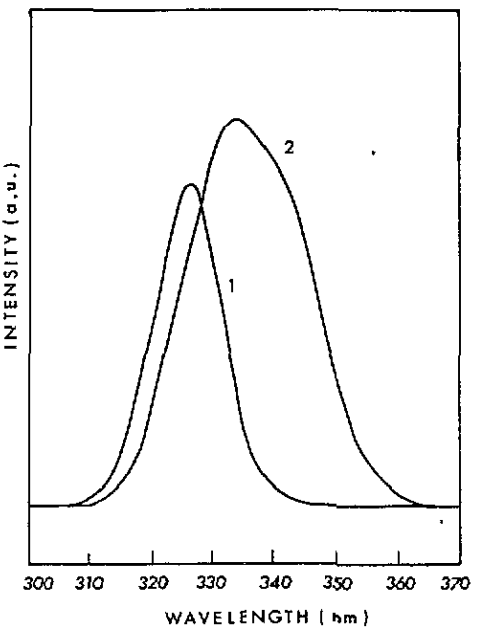

Figure 3. Excitation spectra of the 388 nm (1) and 430 nm (2) emission from KCl:Bi^{3+} measured at $T = 16$ K.

The effect of temperature on the A emission from KCl:Bi^{3+} excited at 326 and 334 nm was also investigated. As shown in figure 4(*a*), at $T = 15$ K the high-energy emission is produced strongly by the 326 nm excitation. As the temperature increases, the intensity of the high-energy emission decreases, and at $T = 30$ K it becomes weaker than that of the low-energy emission. As shown in figure 4(*b*), the low-energy emission produced strongly by the 334 nm excitation is also quenched by the temperature. The 430 nm emission, however, persists up to room temperature. It was found that there is no evidence for non-radiative transitions between the two emitting centres.

Time-resolved emission spectra from KCl:Bi^{3+} excited by N_2 laser were measured at $T = 15$ K. Figure 5 shows the time-resolved spectra from KCl:Bi^{3+} recorded in two different time ranges after the excitation. The strong high-energy emission peaking at 405 nm was observed only for a short time delay after the excitation, while the weak low-energy emission

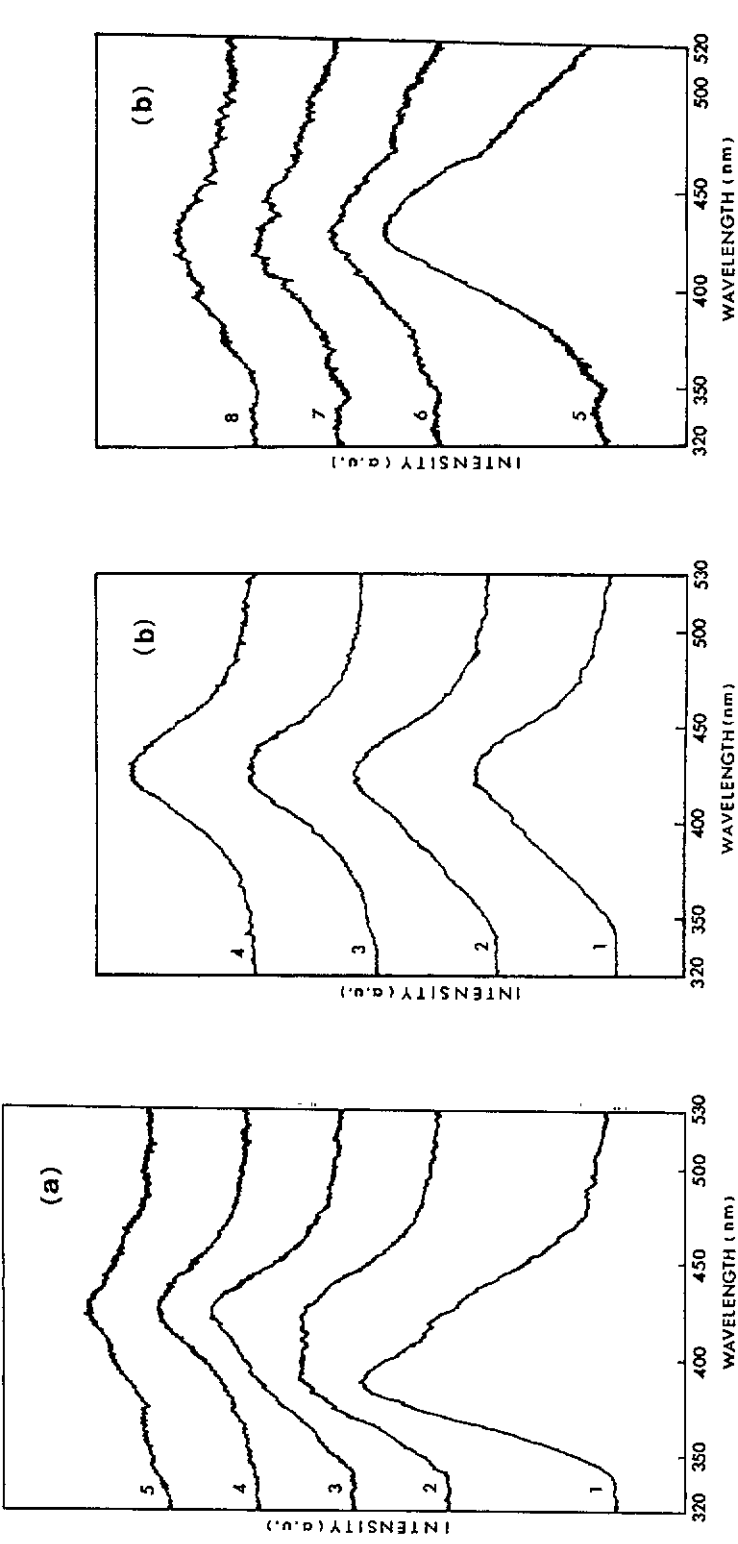

Figure 4. Emission spectra from $KCl:Bi^{3+}$ measured at various temperatures: (*a*) $\lambda_{exc} = 326$ nm and $T = 15$ K (1), 20 K (2), 25 K (3), 30 K (4) and 253 K (5); and (*b*) $\lambda_{exc} = 334$ nm and $T = 15$ K (1), 20 K (2), 25 K (3), 30 K (4), 78.8 K (5), 120 K (6), 150 K (7) and 243 K (8) (the spectra numbered from 5 to 8 were amplified twice as much as the others).

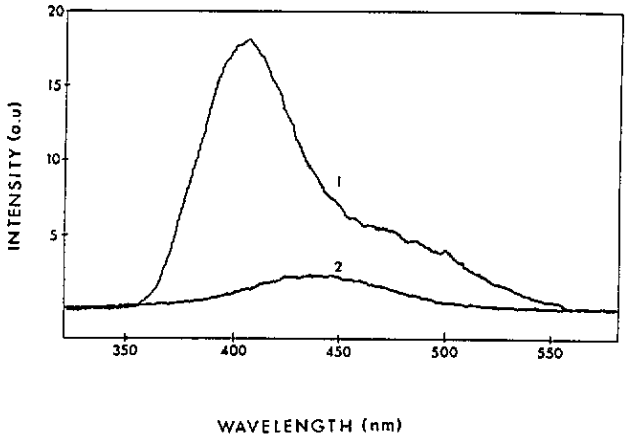

Figure 5. Time-resolved emission spectra from KCl:Bi^{3+} excited by N_2 laser in the time ranges $0 < t < 100$ μs (1) and $300 < t < 700$ μs (2) at $T = 20$ K.

peaking at 440 nm is observable for short and long time delays. Shift of peak positions of both emissions could arise from the weak resolving power of the polychromator used in this measurement. These spectra, however, indicate that the high-energy emission has only a fast decay, while the low-energy emission has both fast and slow decays. The decay curves of the two emission bands were also measured at various temperatures. The lifetimes of both emissions evaluated from the decay curves are shown in figure 6. Below $T = 50$ K, the slow component of the low-energy emission is independent of temperature but decreases rapidly above 50 K, while the fast component of the high-energy emission is almost independent of temperature. A fast component of the decay for the low-energy emission seems to appear. However, it is very difficult to evaluate the short lifetime owing to the overlapped strong high-energy emission band.

3.3. Polarization

The intensity spectra of the A-band emission from KCl:Bi^{3+}, polarized parallel and perpendicular to the direction of the electric vector of the exciting light, were also measured at $T = 16$ K. As shown in figure 7, no further splittings of the A emission band are observed, but a change in the intensity is found. Independently of the exciting photon energy, the intensity of the high-energy emission polarized parallel (A_Π) is stronger than that polarized perpendicular (A_Σ), while for the low-energy emission the intensities of the A_Π and A_Σ spectra are the same. According to the results of KCl:Sb^{3+} (Choi *et al* 1991), for the high-energy emission (assigned as the A_T emission), doublet-shaped A_Π and bell-shaped A_Σ spectra were observed, while for the low-energy emission (assigned as the A_X), the A_Π and A_Σ spectra were found to be equivalent. Between the two phosphors, we found a similarity for the low-energy emission and a difference for the high-energy emission.

Figure 8 shows the angular dependence of polarization ratio of the 388 and 430 nm emissions from KCl:Bi^{3+} measured in the perpendicular geometry at $T = 16$ K. Independently of the angle of the electric vector of the exciting light, the 430 nm emission is totally depolarized and the 380 nm emission shows positively constant values. It indicates that the A-band emission from KCl:Bi^{3+} is not correlated with any preferential symmetry axes.

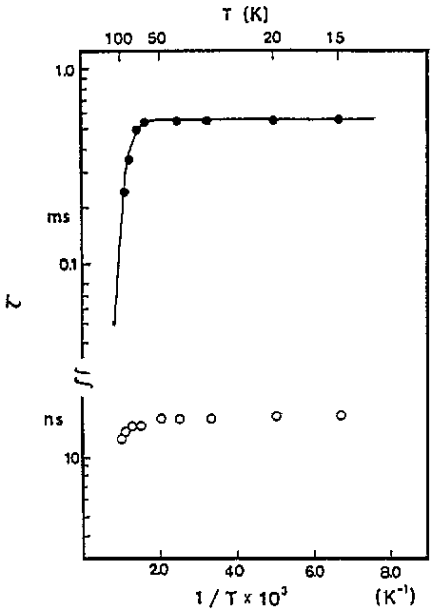

Figure 6. Temperature dependence of the decay times of the low-energy emission (●) and the high-energy emission (O) from KCl:Bi^{3+} excited by N_2 laser.

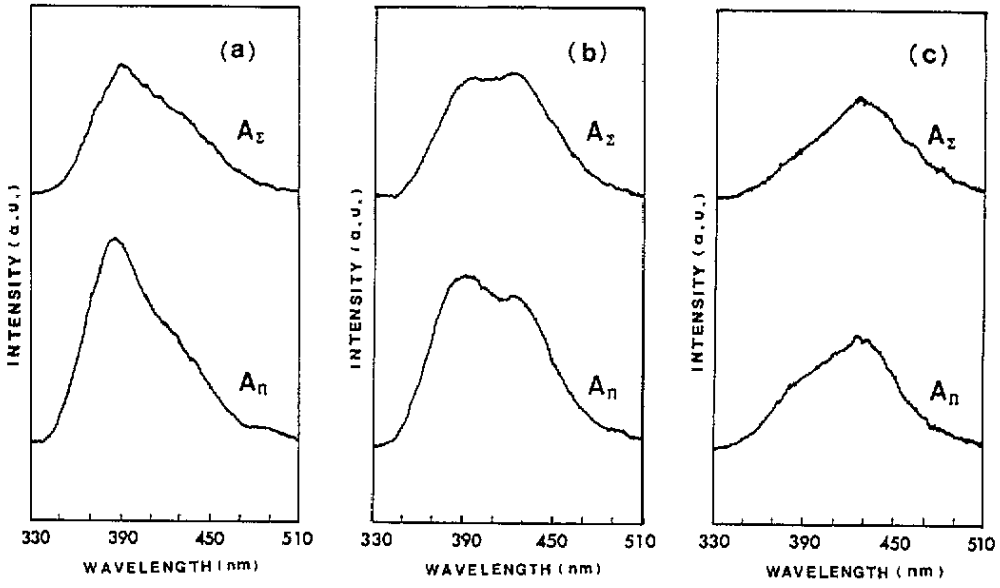

Figure 7. Polarized emission spectra from KCl:Bi^{3+} measured at $T = 16$ K: $\lambda_{exc} = 326$ nm (*a*), 330 nm (*b*) and 334 nm (*c*). The A_Π is the parallel polarized emission spectrum with both the polarizer and the analyser set at $\alpha = 0°$ and $\beta = 0°$ from the z axis, respectively; and the A_Σ is the perpendicularly polarized emission spectrum with $\alpha = 0°$ and $\beta = 90°$.

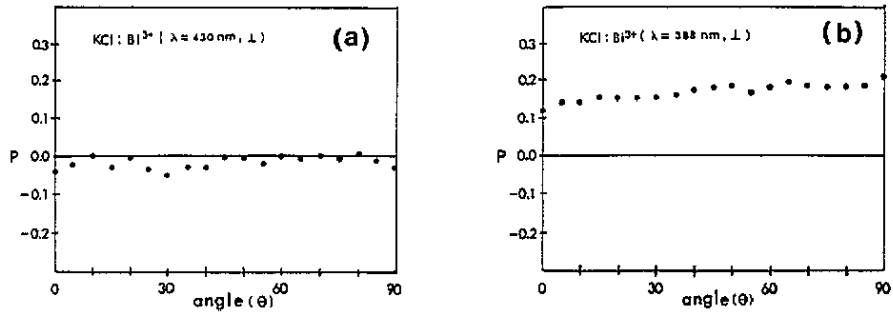

Figure 8. Angular dependence of polarization ratio of (*a*) the 430 nm and (*b*) the 388 nm emissions from KCl:Bi^{3+} in the perpendicular geometry (T = 16 K).

4. Discussion

For the RES accounting for the A-band emission from KCl:Bi^{3+}, we shall discuss the energy-level scheme of the $^3T_{1u}$ in terms of the JTE, the SO interaction and the CCV. Although the $^3A_{1u}$ state is also involved in the processes of the A-band emission, this state is unaffected by the Jahn–Teller and the spin-orbit interactions. Since the metastable $^3A_{1u}$ level is not degenerate, the JTE and the spin-orbit reduction are absent in this level.

4.1. Effects of SO interaction, JT coupling and CCV on the RES of the isolated Bi^{3+} centre

First of all, we shall evaluate the spin–orbit coupling constant ζ and the ratio R of the dipole strength of the C band to that of the A band from the absorption spectrum. According to the energies of the A, B and C bands (Fukuda 1964), ζ can be expressed as $-2a/3 + (6b^2 - 2a^2)^{1/2}/3$, where $a = (E_C + E_A)/2 - E_B$ and $b = (E_C - E_A)/2$. Letting $c = (E_B - E_A)/(E_C - E_A)$, then

$$R = \mu^2/\nu^2 = \{2 - c + [1 + 2c(1-c)]^{1/2}\}/\{1 + c - [1 + 2c(1-c)]^{1/2}\}.$$

Substituting the observed energy values into the formulae, we obtain ζ = 1.074 eV and R = 7.03. The SO interaction of Bi^{3+} in KCl single crystals is exceptionally strong, compared with Tl^+-like ions; for example, ζ = 0.367 for KCl:Ge^{2+} (Lushchik *et al* 1960), 0.36 eV for KCl:Ga^+, 0.278 for KCl:In^+, 0.53 for KCl:Sn^{2+}, 0.692 for KCl:Tl^+, 0.97 for KCl:Pb^{2+} (Honma 1974) and 0.953 for KCl:Sn^{3+} (Tsuboi *et al* 1992). Assuming that the Jahn–Teller energy E_{JT} is approximately equal to half the Stokes shift, E_{JT} = 0.304 eV for the 388 nm emission and E_{JT} = 0.414 for the 430 nm emission. For KCl:Bi^{3+}, the SO interaction is much stronger than the JTE. Therefore, the SO interaction should be treated as the zero-order approximation, while the JTE is regarded as an additive correction.

When the SO interaction is much stronger than the JTE, the three components of the excited $^3T_{1u}$ state may be expressed as a linear combination of states transforming like x, y and z as follows:

$$\begin{aligned} |T_{1u,x}\rangle &= (|Y_-\Theta_z\rangle - |Z_-\Theta_y\rangle)/\sqrt{2} \\ |T_{1u,y}\rangle &= (|Z_-\Theta_x\rangle - |X_-\Theta_z\rangle)/\sqrt{2} \\ |T_{1u,z}\rangle &= (|X_-\Theta_y\rangle - |Y_-\Theta_x\rangle)/\sqrt{2} \end{aligned} \tag{1}$$

where X_- is an antisymmetrized orbital wavefunction given by

$$X_- = [a_{1g}(1)t_{1u,y}(2) - t_{1u,x}(1)a_{1g}(2)]/\sqrt{2} \tag{2}$$

and Y_- and Z_- are similarly expressed. The triplet spin functions are also associated with x, y and z directions as follows:

$$\Theta_x = -[\alpha(1)\alpha(2) - \beta(1)\beta(2)]/\sqrt{2}$$
$$\Theta_y = i[\alpha(1)\alpha(2) + \beta(1)\beta(2)]/\sqrt{2}$$
$$\Theta_z = [\alpha(1)\beta(2) + \beta(1)\alpha(2)]/\sqrt{2}.$$

Since the SO interaction is strong, the off-diagonal elements of the SO interaction between the $^3T_{1u}$ and $^1T_{1u}$ states cause considerable mixing of these two states and leads to the $^3T^*_{1u}$ and $^1T^*_{1u}$ states. The triply degenerate $^3T^*_{1u}$ and $^1T^*_{1u}$ states are stabilized and unstabilized in energy by the mixing, respectively. These states are an appropriate choice for the RES in the zero-order approximation.

The next step is to consider the effect of the JT interaction on the threefold $^3T^*_{1u}$ state. In general, two kinds of vibrational modes, i.e. the tetragonal $E_g(Q_2, Q_3)$ and the trigonal $T_{2g}(Q_4, Q_5, Q_6)$ modes, have been considered for the JT stabilization. If the JT coupling to the trigonal T_g modes is predominant, transitions from the singlet state to the threefold state reveal a three-hump spectrum. This $T \otimes T_{2g}$ problem can account for the C band having triplet structure. For the A-band emission, the $T \otimes E_g$ problem has been taken into account as the main JT effect.

When the linear JT interaction with the $E_g(Q_2, Q_3)$ modes takes place predominantly along the z axis, i.e. $\langle 001 \rangle$ direction, the orbital $|Z_-\rangle$ state becomes more stable than the $|X_-\rangle$ and $|Y_-\rangle$ states. Since the $^3T_{1u,z}$ state is a linear combination of the antisymmetrized $|X_-\rangle$ and $|Y_-\rangle$ states as well as the triplet spin states, the JT distortion splits the $^3T_{1u,x}$ and $^3T_{1u,y}$ states to lower energy and the $^3T_{1u,z}$ state to higher energy through the stabilization of the electronic $|Z_-\rangle$ state. Accordingly, the coupling to the tetragonal E_g modes may split the $^3T^*_{1u}$ state into a double degenerate state with E symmetry at lower energy and a singlet state with A symmetry at higher energy (see figure 9(a)). Analogously, the JT distortion along the x or y axes splits the triply degenerate state into the A state and the E state.

According to the APES of the $^3T^*_{1u}$ state (Ranfagni and Viliani 1974, Mugnai *et al* 1982), two kinds of minima, two X (rhombic) and one T* (tetragonal), can coexist if and only if the SO interaction is of suitable value compared with the JTE coupling to the tetragonal $E_g(Q_2, Q_3)$ mode. Previously, we examined how the two kinds of minima on the APES of the stabilized state with E symmetry are affected by the SO interaction (Choi *et al* 1991). The theoretical calculation for the APES of the state shows that the depth of the T* minimum is significantly affected by the SO interaction, when the SO interaction is strong. In our model, the JT coupling constants b for the E_g modes are modified by introducing the ratio of the dipole moment of the C band to that of the A band, $R(= \mu^2/\nu^2)$. Figure 10(a) shows the effect of the R value on the cross sections of the $^3T^*_{1u,z}$ calculated along the lines passing through one of the two X minima and T* minimum from the origin. When R is not less than 50 (i.e. the SO interaction is of suitable value, compared with the JTE), the X and T^*_z minima can coexist as stationary points on $^3T^*_{1u,z}$ APES. When $R \leqslant 50$, i.e. the SO interaction is strong, the depth of the T^*_z minimum is significantly affected by the SO interaction. Since the value of R for $KCl:Bi^{3+}$ is found to be 7.03, it can be expected that, among the two kinds of minima on the APES of the lower twofold E state, the X minima remain as stationary points and the T* minima can be collapsed to a saddle point.

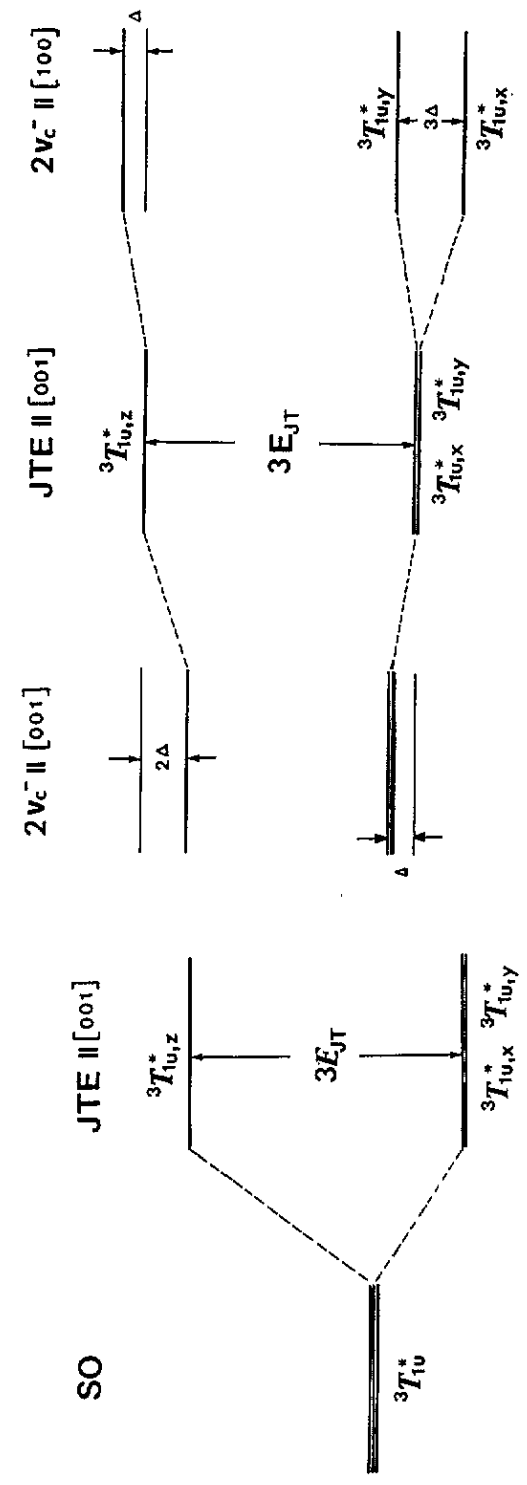

Figure 9. Energy-level scheme of the Bi^{3+} RES: (*a*) the spin–orbit interaction and the Jahn–Teller effect coupling to the E_g mode in the zero-order approximation, and (*b*) the perturbing two cation vacancies in the NNN position.

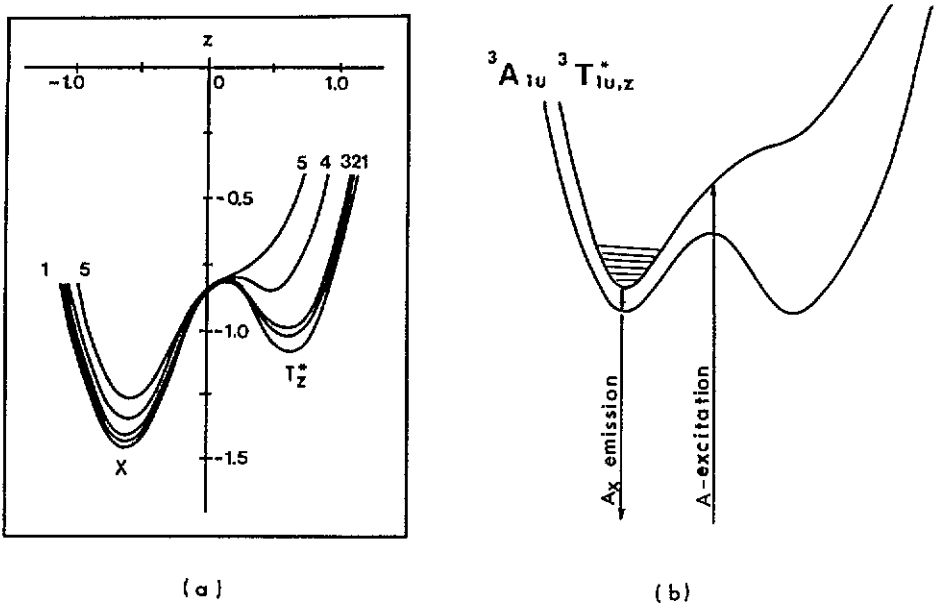

Figure 10. (*a*) Cross sections of the $^3T^*_{1u,z}$ APES along the line connecting one of the X minima and the T_z^* minimum through the origin. Equation (4) is computed for $A = 3$, $g = 0.2$ and several values of $R(\mu, \nu)$:(1) $R = \infty(1, 0)$; (2) $R = 100$ (0.9990, 0.0995); (3) $R = 50$ (0.9901, 0.1400); (4) $R = 10$ (0.9535, 0.305); and (5) $R = 5$ (0.9129, 0.4085). (*b*) configurational coordinate diagram for the $^3A_{1u}$ and $^3T^*_{1u}$ states of the Bi^{3+} ion in KCl single crystal.

In addition, the CCV must be taken into account in the RES of $^3T^*_{1u}$ state. The substitution of Bi^{3+} ions into an alkali halide lattice leads to two cation vacancies, each of which may occupy the nearest-neighbour (NN) or the next-nearest-neighbour (NNN) positions. If the t_{1u} orbital of the Bi^{3+} ion is well localized and the CCV carries an effective negative charge, the interaction between the electron cloud of the t_{1u} orbital and the two vacancies in the NNN site along [001] and [00$\bar{1}$] will raise the energy of the $^3T^*_{1u,x}$ and $^3T^*_{1u,y}$ states by an amount Δ and decrease the energy of the $^3T^*_{1u,z}$ state by an amount 2Δ. Figure 9(*b*) shows the effect of two vacancies in the NNN position along the JT axis. In this case, the two lower levels are raised in energy by an amount Δ but still remain degenerate. If two vacancies are located along one of the axes perpendicular to the JT axis, i.e. the x axis, the CCV may split the $^3T^*_{1u,x}$ state to the lower level by an amount 2Δ and the $^3T^*_{1u,y}$ state to the upper level by an amount Δ (see figure 9(*b*)). In other words, when the two vacancies are located on one of the axes perpendicular to the JT axis, the twofold degenerate state is split by 3Δ. A similar calculation can be obtained for two vacancies in the NN position.

4.2. Assignment of the A-band emission

When the X and T* minima coexist on the $^3T^*_{1u}$ APES, these two minima via the A-band excitation could emit two kinds of emission, i.e. A_X and A_{T^*}: the former is attributed to transitions from the X minima and the latter to transitions from the T* minima to the ground state. It has been found that the A_X and A_{T^*} emissions show isotropy and anisotropy, respectively. Figure 10(*b*) shows the configurational coordinate diagram of the $^3A_{1u}$ and $^3T^*_{1u}$ APES of the Bi^{3+} ion, in which the T* minima is a saddle point and the $^3A_{1u}$ well

is lying just below the X minima. Non-radiative transitions between these two wells give rise to two significant pieces of evidence in the A-band emission. When the $^3A_{1u}$ well can be populated via non-radiative transitions, the A_X emission has a long component of decay time and the population becomes depolarized since the $^3A_{1u}$ state is expressed by $(X_x + Y_y + Z_z)/\sqrt{3}$. Accordingly, the low-energy emission band (430 nm) can be assigned to the A_X emission. The high-energy emission band (388 nm), however, could not be associated with the T* minimum since the excitation processes for both are not the same and the 388 nm emission shows isotropy. If the 388 nm emission is attributed to transitions from the T* minimum, it should show anisotropy arising from the JT coupling to the E_g mode. Accordingly, the diagram shown in figure 10(*b*) is very acceptable for the A-band emission from $KCl:Bi^{3+}$.

For the precise assignment for the two A emission bands, the RES perturbed by the CCV should be taken into account. As discussed earlier, the twofold degenerate state stabilized by the JTE can be affected by the two vacancies. Assuming that the T* minimum on the APES of the $^3T^*_{1u}$ state is collapsed to a saddle point, two types of X minima are possible: X_1 minima whose energy is lowered by Δ and X_2 minima whose energy is raised by 2Δ. This could account for the observed double emission. Accordingly, we can assign the 430 and 388 nm emission to the A_{X_1} and A_{X_2} emission, respectively. From this assignment, we obtain $\Delta \simeq 0.104$ eV.

Taking into account all possible relative orientations of the CCV and the JT axes, the circumstances may cause the weight of the X_2 minima to be twice as much as that of the X_1 minima. As the value of Δ increases, the positions of the two X_2 minima on the APES of each level should be away from the trap but close to the origin. Consequently, they could form a trigonal configuration. This assumption is a valid explanation for the results of the decay with only short component and the isotropy of the 388 nm emission.

4.3. Decay kinetics of the 430 nm emission

We consider the kinetics of the luminescence decay of the A_{X_1} band. As a result of the RES, a three-level system is required as shown in figure 11, in which level 2 represents the X_1 state, level 1 the $^3A_{1u}$ state and level 0 the ground state. As the selection rule, the X_1 level is populated by the pulse excitation of the A absorption band, followed by non-radiative transitions to the $^3A_{1u}$ well lying as a trap. Transitions from level 1 to the ground state (0) originating from level 2 yield the slow component and transitions from level 2 to level 0 possibly produce the fast component.

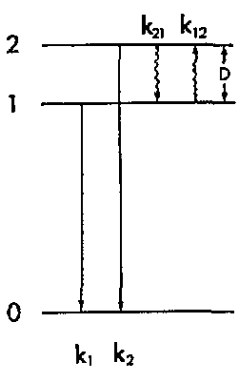

Figure 11. Three-level system for the decay kinetics for the 430 nm emission from $KCl:Bi^{3+}$.

In figure 11, k_i $(i = 1, 2)$ corresponds to the radiative transition probability from level i to the ground state, and k_{ij} $(j = 1, 2)$ corresponds to the non-radiative transition probability from level i to level j. If one phonon is involved in the non-radiative transitions between the RES, then the non-radiative and reverse non-radiative transitions are described as follows:

$$k_{21} = Kn \qquad k_{12} = K(n+1) \tag{4}$$

where K is a constant and n is the Bose–Einstein distribution given by

$$n = 1/[\exp(D/kT) - 1] \tag{5}$$

and D is the energy separation between the upper two levels.

Assuming that the non-radiative transitions between the X_1 and X_2 wells is negligible, two rate equations for levels 2 and 1 are obtained:

$$\begin{aligned} \mathrm{d}N_2/\mathrm{d}t &= -(k_2 + k_{21})N_2 + k_{12}N_1 \\ \mathrm{d}N_1/\mathrm{d}t &= k_{21}N_2 - (k_1 + k_{12})N_1 \end{aligned} \tag{6}$$

where N_i is the population of level i. Provided that the rate equation for the population of level i has a decay time of the form

$$\sum C_i \exp(-t/\tau_i)$$

where C_i is a constant and τ_i is a decay time, the corresponding matrix is:

$$\begin{pmatrix} 1/\tau - (k_2 + k_{21}) & k_{12} \\ k_{21} & 1/\tau - (k_1 + k_{12}) \end{pmatrix} = 0. \tag{7}$$

The solutions of equation (7) result in two decay times for any given temperature as follows:

$$\tau_s = \{[-A - (A^2 - 4B)^{1/2}]/2\}^{-1} \tag{8a}$$

$$\tau_f = \{[-A + (A^2 - 4B)^{1/2}]/2\}^{-1} \tag{8b}$$

where $A = -(k_2 + k_{21} + k_1 + k_{12})$ and $B = (k_1k_2 + k_2k_{12} + k_1k_{21})$. In equation (8), τ_s and τ_f belong to the slow and fast components of the decay times, respectively.

The observed time-resolved spectrum of the A_{X_1} band exhibits both long and short components of the emission decay. The fast component of the A_{X_1} band, however, is unacceptable owing to weak intensity and overlap with the fast component of the strong A_{X_2} band. We focus our attention on the slow component, τ_s.

At low temperature, if $D \gg kT$, then $k_{12} \simeq 0$, i.e. the reverse non-radiative processes from level 1 to level 2 could not occur. When $k_2 \gg k_1$, equation (8*a*) becomes

$$1/\tau_s \simeq k_1. \tag{9}$$

It shows that the decay time of the trap, τ_s, corresponds to the limiting value of the low-temperature plateau. As the temperature increases, the reverse non-radiative process increases but is still very small compared with the non-radiative process. In the intermediate temperature range, if $k_2k_{12} > k_1k_{21}$, then equation (8*a*) gives

$$1/\tau_s \simeq nk_2K/[k_2 + K(n+1)]. \tag{10}$$

If $\exp(D/kT) \gg 1$, i.e. $n \ll 1$, equation (10) is simplified to

$$\tau_s \simeq [(K + k_2)/Kk_2] \exp(D/kT). \tag{11}$$

Equation (11) shows that in the intermediate temperature range a plot of the logarithm of the slow decay time versus $1/T$ is linear with a slope of D/k.

Values of the parameters in equation (8*a*) were chosen to give the best fit to the temperature dependence of the slow decay time. The results are

$$k_1 = 1.85 \times 10^3 \text{ s}^{-1} \qquad k_2 = 6.25 \times 10^7 \text{ s}^{-1}$$

$$K = 5.0 \times 10^6 \qquad D = 0.059 \text{ eV}.$$

The slow decay time from the solution of equation (8*a*) is plotted as the full curve in figure 6. One can see that the theoretical values coincide well with the experimental ones.

5. Conclusion

The spin–orbit coupling constant of Bi^{3+} in KCl single crystals obtained from the absorption spectrum is about 1.07 eV, which is exceptionally strong, compared with Tl^+-like ions. The strong SO interaction lowers the three equivalent RES of $^3T_{1u}$ equally via mixing with the $^1T_{1u}$ state. Coupling to the E_g mode splits these reduced RES into a twofold degenerate state with E symmetry at lower energy and a singlet state with A symmetry at higher energy. The strong SO interaction, however, could reduce the JT stabilization coupling to the E_g mode. Consequently, of the two kinds of minima, X and T*, on the APES of the $^3T^*_{1u}$, the T* may collapse to a saddle point, while two X minima on each APES still remain as stationary points.

In general, the effect of the cation vacancy is not strong enough to split the A emission band except in the case of Sn^{2+} but is treated as an additional perturbation. The lower-energy E state, however, may be further split depending on the relative orientation of the two vacancies and the JT axes. If the two vacancies are along the JT axes, the E state is raised in energy by an amount Δ, but still remains degenerate. Otherwise, the twofold degenerate state is split by 3Δ. Under these circumstances, there are two types of X minima: one is the lowered X_1 and the other is the raised X_2 minima. The 430 and 380 nm emissions can be attributed respectively to the transition from the X_1 and from the X_2 minima to the ground state. This assignment explains well the observed experimental results for the two A emission bands.

Acknowledgments

This work was supported by the Korean Research Foundation (KRF). TT would like to thank KRF for the grants of the visiting program.

References

Choi K O, Lee S W, Bae H K, Jung S H, Chang C K and Kang J G 1991 *J. Chem. Phys.* 94 6420
Fukuda A 1964 *Sci. Light* **13** 64
—— 1970 *Phys. Rev.* B **1** 4161
Höner J, Siederdissen Zu and Fischer F 1971 *Phys. Status Solidi* b **48** 215
Honma A 1974 *Sci. Light* **23** 43
Hughes A E and Pells G P 1975 *Phys. Status Solidi* b **71** 707
Kang J G, Cusso F, Belliveau T F and Simkin D J 1985 *J. Phys. C: Solid State Phys.* **18** 4753
Kang J G, Ju S K, Gill Y H, Shim I K and Chang C K 1988 *J. Phys. Chem. Solids* **49** 813
Lushchik Ch B, Liidvya G G, Lushchik N E, Shvarts K K and Yaek I V 1960 *Sov. Phys.–Solid State* **3** 855
Mugnai D, Ranfagni A and Viliani G 1982 *Phys. Rev.* B **25** 4284
Onaka R, Fukuda A and Mabuchi T 1965 *J. Phys. Soc. Japan* **20** 466
Radharkrishna S and Srinivasa Setty R S 1976 *Phys. Rev.* B **14** 969
Ranfagni A and Viliani G 1974 *J. Phys. Chem. Solids* **35** 25
Schmitt K 1982 *Phys. Status Solidi* b **113** 559
Seitz F 1938 *J. Chem. Phys.* **6** 150
—— 1939 *Trans. Faraday Soc.* **35** 74
Tsuboi T, Ahmet Pand Kang J G 1992 *J. Phys.: Condens. Matter* **4** 531
Tsuboi T and Silfsten P 1991 *Phys. Rev.* B **43** 1135